JOURNAL OF MATERIALS SCIENCE 20 (1985) 1953–1960

Silicon carbide filaments: microstructure

S. R. NUTT*
Metallurgy Division, National Bureau of Standards, Washington, DC, USA
F. E. WAWNER
Department of Materials Science, University of Virginia, Charlottesville, VA, USA

The microstructure of chemically vapour deposited silicon carbide filaments has been examined using transmission electron microscopy. The filament bulk consisted of heavily faulted columnar subgrains of β-SiC which were preferentially oriented such that {1 1 1} planes were parallel to the surface of the carbon fibre substrate. The protective coating on the filament surface was characterized by several microstructurally distinct layers, all of which consisted primarily of carbon. The first layers of the coating contained small crystallites of SiC in addition to turbostratic carbon, while the outer layers showed no evidence of SiC. Implications of the filament microstructure with respect to mechanical properties are discussed.

1. Introduction

Silicon carbide filaments are of considerable interest as reinforcements for metal matrix composites. They exhibit excellent mechanical and physical properties, including a high specific strength and modulus [1]. Temperatures up to 800° C have no appreciable effect on these properties [2, 3], making SiC a prime candidate for high-temperature applications. In addition, the relatively large diameter of the filaments facilitates composite fabrication by liquid metal infiltration and enhances impact resistance [4]. Unfortunately, the use of SiC filaments in composite structures has evolved slowly. This is primarily due to technical problems (such as interfacial reactions and filament cracking) encountered during fabrication and processing of composites [5]. These problems are undoubtedly related to microstructural features of the filaments which arise from the method of production.

Silicon carbide filaments are produced by chemical vapour deposition (CVD) [6]. In this process, a 33 μm diameter carbon pitch fibre is pulled continuously through a deposition tube while being electrically heated. Silane vapours are introduced into the tube through two inlets and the hot carbon substrate catalyses the decomposition of silane molecules [7]. Columnar grains of β-SiC deposit on the carbon fibre and grow radially out from the substrate [6, 7]. Adjacent columnar grains of CVD SiC typically exhibit small misorientations and are often referred to as subgrains [8–10].

The resulting filament, like most high-strength high-modulus reinforcements, is brittle and exhibits a distribution of strengths. The filament is extremely sensitive to surface defects and abrasion. To overcome this problem, the filament manufacturers† have recently developed a protective carbon–silicon coating called "SCS", which is also applied by CVD. The coating reportedly consists mostly of carbon and is slightly enriched in silicon at the surface [11–13]. The presence of the SCS surface layer causes a twofold increase in filament strength [6, 14], presumably by reducing the severity of stress concentration at the filament surface.

In this investigation, the internal microstructure of SCS SiC filaments is studied using transmission electron microscopy (TEM). Particular attention is focused on the SCS surface layer because of its critical importance in promoting filament strength

*Currently at Arizona State University, Center for Solid State Science, Tempe, Arizona, USA.
†AVCO, Speciality Materials Division, Lowell, Massachusetts, USA.

0022–2461/85 $03.00 + .12

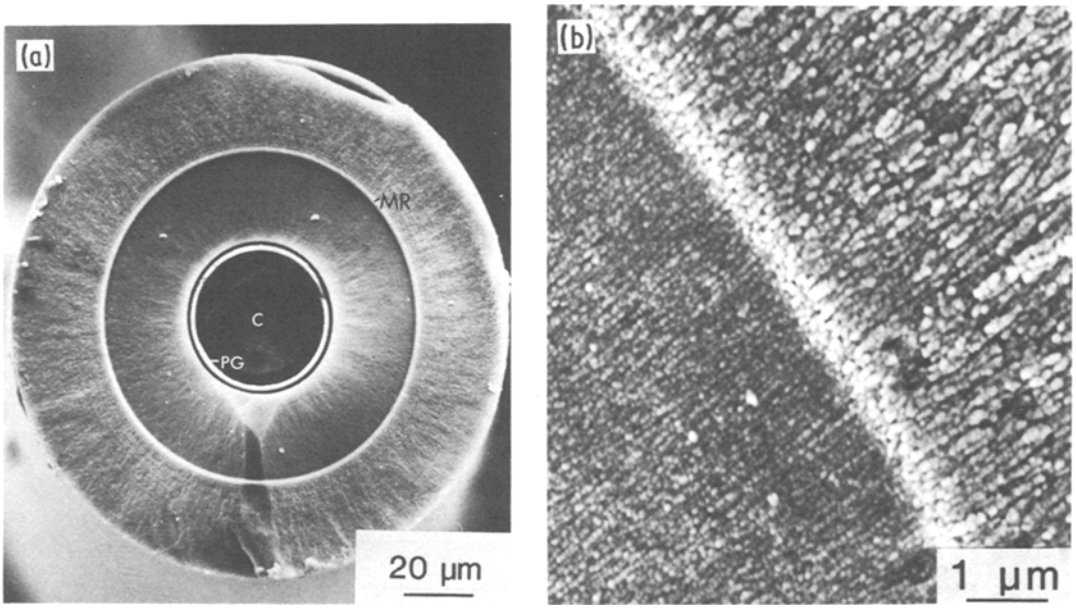

Figure 1(a) An etched SiC filament grown by CVD on a carbon wire (C) with a pyrolytic graphite layer (PG). (b) Enlargement of midradial region (MR) showing a change in the diameters of SiC subgrains

and in protecting the filament from undesirable reactions with metal matrices.

2. Experimental procedure

Continuous filaments of silicon carbide‡ were obtained from a commercial source†. The microstructure of bulk filaments was first examined in a scanning electron micrscope (SEM). SEM specimens were prepared by etching filament ends in a molten salt mixture of KOH and KNO_3 for 3 to 5 min [15], followed by rinsing and ultrasonic cleaning in solvents.

The preparation of TEM specimens was accomplished by a technique similar to the one first reported by Shaw [16]. A single layer of parallel SiC filaments was placed between two foils of 1100 (commercial purity) aluminium. The assembly was then diffusion-bonded in an argon atmosphere at 550° C for 30 min to produce a composite monotape. Wafers 4 mm square were sectioned from the monotape and mechanically polished from both sides to a final thickness of 50 μm. An ultrasonic core drill was then used to cut discs 3 mm in diameter. Discs were finally ion-thinned to perforation using an argon-beam ion mill operating at 6 kV, 50 mA per gun, and 15° to 20° incidence angle.

‡Trade name "SCS–2".
†AVCO, Specialty Materials Division, Lowell, MA.

3. Results and discussion

3.1. Filament microstructure

The microstructure of SCS SiC filaments is revealed in scanning electron micrographs of etched filament ends (Fig. 1). A thin layer of pyrolytic graphite (PG) is present on the surface of the original carbon fibre to provide a uniformly smooth surface for the deposition of SiC. Columnar subgrains of SiC grow radially outward from this PG layer to a final filament diameter of 142 μm. The term "subgrains" here is used to refer to adjacent grains of small crystallographic misorientation, as will be shown later, and is not meant to imply polygonization or recovery. The nodular morphology of the subgrains is attributed to curvatures of the subgrain boundaries and to preferential etching at sites of extreme stacking disorder [15]. Another salient feature is the pronounced midradial (MR) boundary located 22 μm from the PG layer on the carbon wire. Outside the MR boundary, subgrains are approximately 0.1 μm in diameter, while inside they are considerably smaller. This marked change in grain diameter is caused by a sudden change in growth conditions at the second inlet to the deposition chamber. The supersaturation of silane

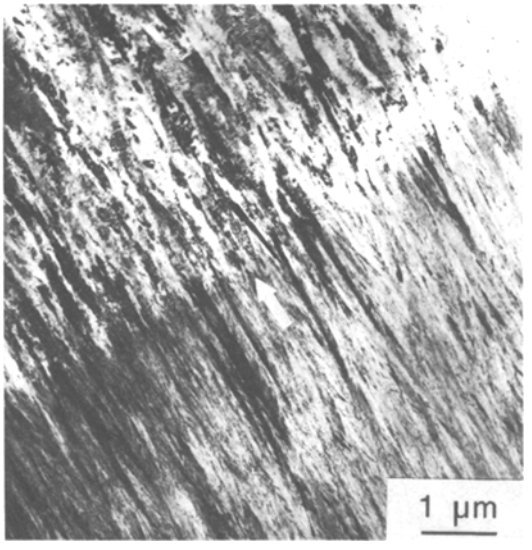

Figure 2 TEM micrograph showing columnar subgrains of SiC at the midradial boundary of the filament. The arrow indicates the growth direction.

vapours is presumably lower at the second inlet, causing a slightly lower nucleation density and larger subgrain diameter [7].

The internal microstructure of the MR region is shown in the TEM micrograph in Fig. 2. Subgrain widths are 40 to 50 nm inside the MR boundary and 90 to 100 nm outside. Subgrain lengths range up to a few micrometres, although it is difficult to distinguish points of termination. Slight misorientations between subgrains are evident, as well as apparent curvatures of subgrain boundaries.

Electron diffraction patterns from the regions shown in Fig. 2 exhibit intense {1 1 1}β reflections that are arc-shaped (Fig. 3). The arcs indicate a strongly preferred orientation of the SiC subgrains in which close-packed {1 1 1} β planes lie perpendicular to the radial growth directions. Misorientation between adjacent subgrains ranges from 0 to 17°, giving rise to the arc shapes of the different reflections. Streaking is also apparent in the pattern (region marked S), caused by extensive planar disorder within the subgrains. Planar disorder appears in the image as fine parallel bands running across the subgrains (Fig. 2). Interplanar spacings calculated from the patterns confirm that the crystal structure is that of cubic (β) SiC. Small differences in the appearance of patterns from inside and outside the MR boundary are attributed to the different subgrain sizes in the two regions.

Fig. 4 shows a typical subgrain of SiC containing a high density of narrow {1 1 1} twins and stacking faults. The subgrain is in a ⟨1 1 0⟩ orientation so that {1 1 1} planes (and twins) are viewed "edge-on" in the micrograph. The twin lamellae run completely across the subgrain diameter and vary in width up to 45 nm. The distribution of twin widths results from the growth process which apparently involves a nearly random nucleation of layers. The corresponding [1 1 0] convergent beam diffraction pattern shows additional diffracted disks from the twins as well as streaking due to the planar disorder.

Considerable planar disorder is common in silicon carbide [8, 17], partly because of the very low stacking fault energy of {1 1 1} β or {0 0 0 1} α planes [18, 19]. Stacking defects reportedly involve 180° rotations of SiC tetrahedra about the [1 1 1] axis [12, 20]. Regular arrangements of the

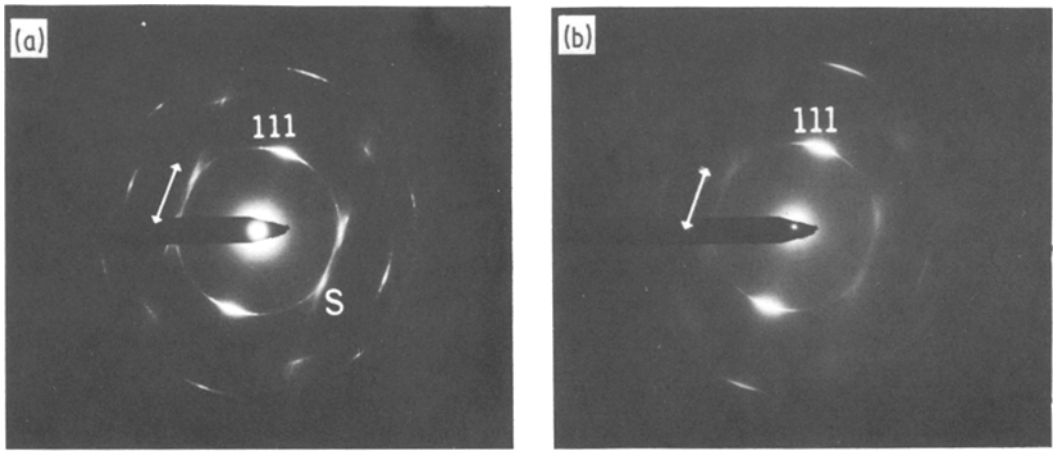

Figure 3 Selected area diffraction patterns from outside (a) and inside (b) the midradial boundary shown in Fig. 2. Arcs indicate preferred orientation and streaks (S) indicate stacking disorder. The growth direction is parallel to the arrow.

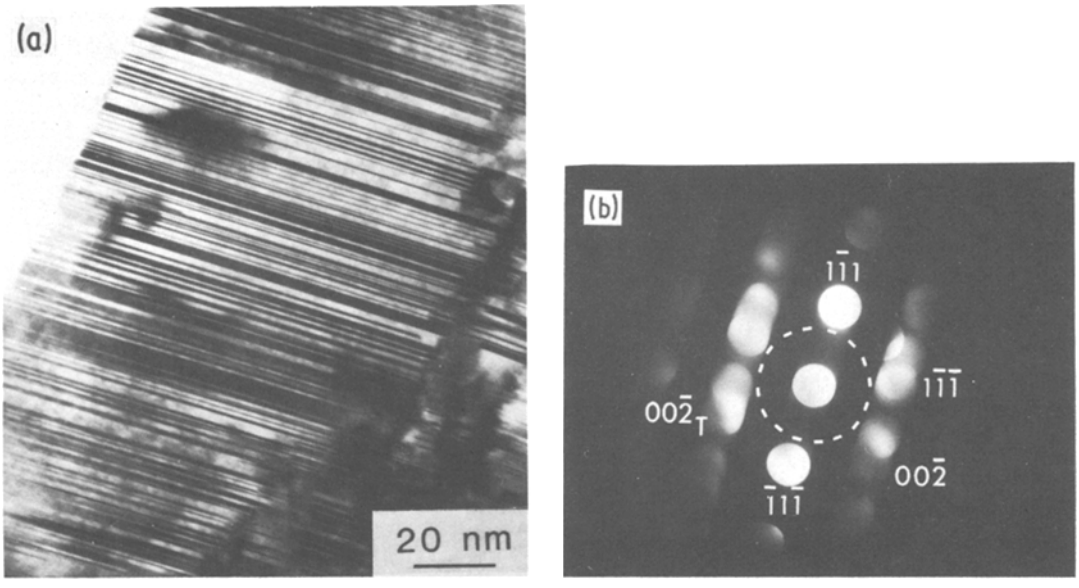

Figure 4(a) Subgrain of SiC from outside the MR boundary of a CVD SiC filament, viewed in the [1 1 0] direction. Narrow {1 1 1} twins and stacking faults give rise to the diffraction contrast. (b) A convergent beam diffraction pattern from the disordered subgrain, showing the position of the objective aperture used in (a).

stacking faults (or layers of rotated and non-rotated tetrahedra) give rise to different SiC structures called polytypes [21]. The structure of the subgrain in Fig. 4 is predominantly β-phase, the cubic polytype, although the subgrain also includes many lamellar twins. The narrowest of these twin lamellae measure approximately 0.25 nm (Fig. 4), corresponding to one or two layers of rotated tetrahedra[§] in the SiC lattice [15].

Silicon carbide crystallites nearest the carbon substrate lack the pronounced columnar morphology exhibited by most of the filament (Fig. 5). The first-deposited SiC crystallites are equiaxed and range in size from 30 to 100 nm. Corresponding selected area diffraction (SAD) patterns exhibit spotty rings of β-SiC with no evidence of preferred orientation. Equiaxed grains are evidently characteristic of the initial stages of the chemical vapour deposition of silicon carbide [10], and the columnar grain morphology does not develop until later in the deposition process.

3.2. SCS coating

The SCS coating on SiC filaments is characterized by multiple layers. The first layer of the coating is deposited on a sawtooth-like surface formed by the outermost SiC subgrains of the filament (Fig. 6). The first-deposited material consists of small crystallites of SiC (10 to 40 nm) embedded in a carbon matrix. In the bright-field image (Fig. 6) the SiC crystallites appear as dark spots, while in the dark-field image taken with part of the {1 1 1} β diffracted ring (Fig. 7) they appear light. The corresponding SAD pattern (Fig. 8b) shows broad uniform rings from fine-grained β-SiC as well as a diffuse ring from isotropic randomly oriented pyrolytic carbon [22]. The term "isotropic" here refers to a carbon microstructure without macroscopic growth features. The number and size of the SiC crystallites decrease sharply 0.1 μm from the coating–filament (C–F) interface, where the second layer begins.

The second layer of the SCS coating, located from 0.1 to 1.0 μm from the bulk filament, is a transition region which is predominantly carbon. In this layer, the carbon becomes preferentially oriented and the silicon content gradually decreases to zero. SAD patterns from this region exhibit pronounced broad arcs (Fig. 8c) which are typical of turbostratic pyrolytic carbon [22, 23]. The arcs indicate a preferred orientation in which the {0 0 0 2} layer planes of carbon tend to align parallel to the filament surface. The width of the arcs reflects the extremely small size of the ordered regions, estimated to be 3 to 5 nm. Also

[§] A layer of tetrahedra consists of a layer of carbon atoms and a layer of silicon atoms.

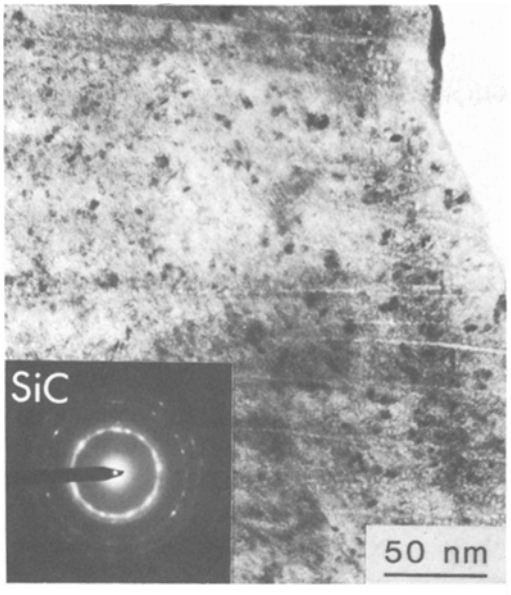

Figure 5 SiC crystallites deposited near the pyrolytic graphite substrate. The equiaxed β-SiC grains range from 3 to 10 nm, and the SAD pattern shows no evidence of preferred orientation.

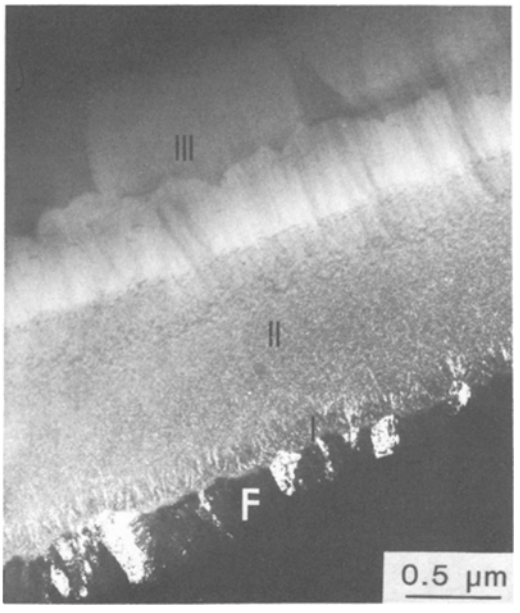

Figure 7 Dark-field image of the SCS coating on SiC filament (F) using {1 1 1} β SiC reflection. Small crystallites of SiC are present in regions I and II, while region III exhibits carbon growth features.

present in the second layer are sparsely distributed crystallites of SiC, visible as bright spots in the dark-field image of Fig. 7. The ultrafine (< 5 nm) SiC grains decrease in number with increasing distance from the filament, and disappear entirely at a distance of 0.7 μm from the C–F interface (Fig. 7).

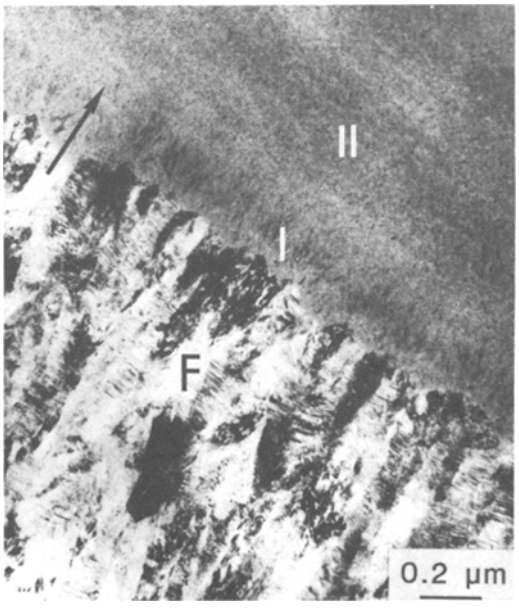

Figure 6 Interfacial region showing the first two layers (I and II) of the SCS coating on the SiC filament (F). The arrow indicates the growth direction.

Of particular interest is the mechanism by which the presence of the SCS coating doubles the strength of SiC filaments. The surface morphology of uncoated CVD SiC filaments resembles the sawtooth interface shown in Figs. 6 and 7. In uncoated SiC filaments, these sawtooth notches concentrate stresses at subgrain boundaries, leading to brittle fractures at low stress levels. In composite materials, the exposed subgrain boundaries lying transverse to the filament axis might provide channels for accelerated diffusion between the matrix and the filament bulk, further decreasing the strength. The SCS coating effectively masks the stress-concentrating notches and provides a smooth transition to a dissimilar material. This reduces the stress intensities associated with the rough surface and eliminates many low stress level failures, thereby increasing the mean strength of the filaments.

The third layer of the SCS coating consists of laminar carbon [23] and is separated from the second layer by a distinct boundary located 1 μm from the C–F interface (Fig. 7). Diffraction patterns from the third layer resemble those of the second layer (Fig. 8c), indicating a similar preferred orientation of {0 0 0 2} layer planes

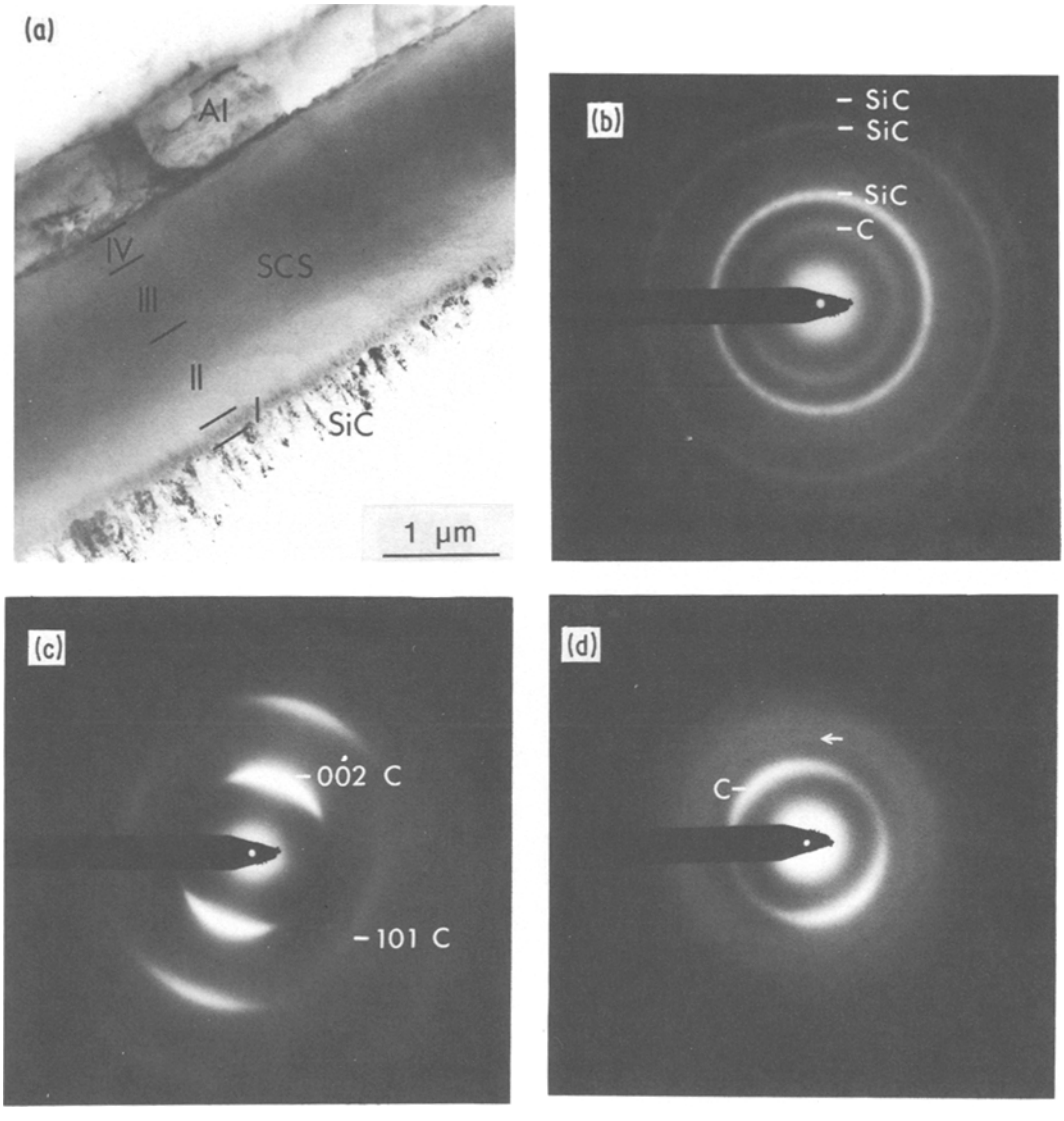

Figure 8 Microstructural variations in the SCS coating. (a) Cross-sectional view showing the SiC filament, layers I to IV of the SCS coating, and the aluminium subgrains. Selected area diffraction patterns from (b) region I, (c) regions II and III, and (d) region IV.

parallel to the deposition surface. However, the appearance of the third layer is quite different, showing large smooth growth features as well as faint striations in the growth direction (Fig. 7). Similar growth features in pyrolytic carbons have been reported [23, 24] as well as a variety of carbon microstructures which depend on reactant gas concentrations and temperature [23]. Thus, the abrupt microstructural transition between the second and third layers is attributed to a sudden increase in the concentration of hydrocarbon gas during deposition.

Near the coating surface, a fourth layer is characterized by a carbon microstructure that is more randomly oriented than the laminar carbon of the third layer. The diffraction pattern (Fig. 8d) exhibits an intense innermost ring that is only slightly arc-like. This ring is attributed to turbostratic carbon [22] with an interplanar spacing of 0.35 nm. Outside the first ring, a weak diffuse ring is visible (see arrow in Fig. 8d) which is not present in the diffraction pattern from the third layer, shown in Fig. 8c. The d-spacing corresponding to the additional ring in Figure 8d is 0.26 nm, a value nearly equal to the interplanar spacings of several SiC polytypes. Previous work

has shown that the outer surface of the SCS coating is enriched in silicon and sometimes contains silicon carbide [12, 13]¶. In this work also, a trace amount of silicon was detected in the outermost fourth layer using X-ray microanalysis in TEM. However, individual crystallites of silicon carbide were not resolvable by conventional TEM imaging (Fig. 9). (The outermost layer of the coating exhibits negligible diffraction contrast and is similar in appearance to the third layer of turbostratic carbon.) The difference in carbon microstructure indicated by the diffraction patterns in Figs. 8c and 8d is thus attributed to the presence of silicon in the outermost coating, perhaps in the form of small ordered regions of SiC dispersed in a predominantly carbon matrix.

The absence of a continuous layer of SiC at the coating surface is particularly important since it is believed that an outer layer of SiC is essential to protect against strength-degrading interfacial reactions in metal–matrix composites. The reaction of primary concern in aluminium matrix composites is the formation of aluminium carbide (Al_4C_3), a water soluble compound which is very deleterious to composite properties [25]. Crystallites of aluminium carbide form at the coating–matrix interface during composite fabrication by diffusion bonding (Fig. 9). The crystallites form on the matrix side of the interface and exhibit a platelet morphology with the largest facets on the basal planes of the hexagonal Al_4C_3 phase. Such intercalation in a composite material would adversely affect mechanical properties and make the material susceptible to environmental attack.

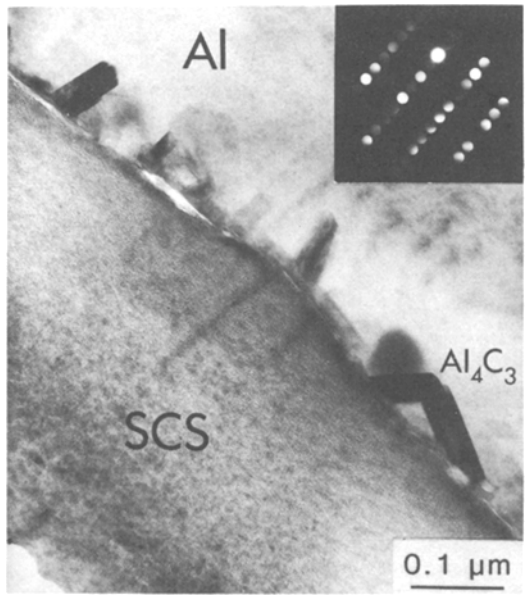

Figure 9 Interface between the SCS coating (C) and the aluminium matrix (Al). Crystallites of aluminium carbide (Al_4C_3) have grown into the matrix during composite fabrication. Inset shows $[2\bar{1}\bar{1}0]$ microdiffraction pattern from Al_4C_3 phase.

4. Summary and conclusions

The microstructure of coated SCS SiC filaments is characterized by heavily-faulted columnar subgrains preferentially oriented such that $\{1\,1\,1\}\beta$ planes lie perpendicular to the radial growth directions. Adjacent subgrains exhibit misorientations ranging from negligible to as much as seventeen degrees. The SCS coating consists of several different layers which are composed mostly of carbon with small amounts of silicon distributed in certain regions. Microstructual differences between the very thin sublayers of the SCS coating indicate a rapidly changing growth environment during the deposition process. The strength-promoting effect of the SCS coating apparently involves the masking of stress-raising notches which occur between adjacent subgrains of SiC.

Acknowledgement

The authors gratefully acknowledge the support of NASA, Lewis Research Center during this work. SRN also thanks the National Research Council for support while writing this manuscript.

References

1. D. M. KOTCHICK, R. C. HINK. and R. E. TRESSLER, *J. Composite Mater.* **9** (1975) 327.
2. K. D. McHENRY and R. E. TRESSLER, *ibid.* **9** (1975) 73.
3. M. W. LINDLEY and B. F. JONES, *Nature* **255** (1975) 474.
4. D. L. McDANIELS and R. A. SIGNORELLI, in *"Failure Models in Composites III"*, edited by T. T. CHIAO and D. M. SCHUSTER (AIME, New York, 1976) p. 27.
5. J. A. CORNIE, R. J. SUPLINSKAS and A. W. HAUZE, in Proceedings of the 4th Annual Conference on Composites and Advanced Materials Cocoa Beach, FL, January 1980 (American Ceramic Society, Columbus, Ohio, 1980) p. 728.
6. R. L. CRANE and V. J. KRUKONIS, *Ceram. Bull.* **54** (1975) 184.

¶There is some variability in the coating surface because of difficulties in achieving uniform deposition parameters.

7. J. R. WEISS and R. J. DIEFENDORF, "Relationship of Structure to Properties of SIlicon Carbide Filament", in Proceedings of the 4th Chemical Vapor Deposition Conference, Boston, MA, October 1973 (Electrochemical Society, Princeton, NJ, 1973). p. 488.
8. S. S. SHINOZAKI and H. SATO, *J. Amer. Ceram. Soc.* **61** (1978) 425.
9. L. U. OGBUJI, T. E. MITCHELL, A. H. HEUER and S. SHINOZAKI, *ibid.* **64** (1981) 100.
10. S. SHINOZAKI and K. R. KINSMAN, *Mater. Sci. Res.* **11** (1979) 641.
11. J. A. CORNIE, Fourth Metal–Matrix Composites Technology Conference, MMCIAC, Santa Barbera, CA, May 1982, pp. 30-1–30-9.
12. S. R. NUTT, PhD dissertation, University of Virginia (1982).
13. S. R. NUTT and F. E. WAWNER, in "Metal Matrix Composites II", NASA Conference Publication 2252 (1982) p. 27.
14. J. A. CORNIE, AVCO Specialty Materials Division, Lowell, MA, private communication.
15. N. W. JEPPS and T. F. PAGE, *J. Microsc.* **124** (1981) 227.
16. G. G. SHAW, in Proceedings of the 29th Annual Meeting of the Electron Microscopy Society of America, Boston, August 1971, edited by C.J. Areeneaux (Claitors, Baton Rouge, 1971) p. 204.
17. S. R. NUTT, *J. Amer. Ceram. Soc.* **67** (1984) 428.
18. R. STEVENS, *J. Mater. Sci.* **7** (1972) 517.
19. T. E. MITCHELL, L. U. OGBUJI and A. H. HEUER, *J. Amer. Ceram. Soc.* **61** (1978) 412.
20. N. W. JEPPS, D. J. SMITH and T. F. PAGE, *Acta Crystall.* **A35** (1979) 916.
21. A. R. VERMA and P. KRISHNA, "Polymorphism and Polytypism in Crystals" (John Wiley and Sons, New York, 1966) p. 76.
22. J. C. BOKROS, in "Chemistry and Physics of Carbon", Vol. 5, edited by P. L. Walker (Marcel Dekker, New York, 1969) p. 1.
23. J. L. KAAE, T. D. GULDEN and S. LIANG, *Carbon* **10** (1972) 701.
24. L. F. COFFIN, *J. Amer. Ceram. Soc.* **47** (1964) 473.
25. W. C. HARRIGAN, *Metall. Trans.* **9A** (1978) 503.

Received 31 January
and accepted 21 June 1984